

Simulation of the SF₆ tracer with the middle atmosphere MAECHAM4 model: Aspects of the large-scale transport

E. Manzini and J. Feichter

Max Planck Institut für Meteorologie, Hamburg, Germany

Abstract. The large-scale transport in a general circulation model is evaluated by analyzing a multiyear simulation that included a passive tracer, with emissions linearly increasing with time, aimed at representing the sources of sulphur hexafluoride, SF₆, a compound of anthropogenic origin. A motivation to analyze the large-scale passive tracer transport is the expected use of such general circulation models in simulations including active feedbacks with chemical models. It has been found that the time evolution and detrended distribution of the simulated SF₆ concentration are comparable to those estimated by available observations of SF₆, both displaying high values in the upper troposphere and low values in the stratosphere. The simulation with a general circulation model of a tracer with surface sources linearly increasing in time and no sinks allows derivation of transport timescales. The age of air from the SF₆ simulation is consistent with the general features of age of air estimates from observations, as, for instance, a rapid increase in age in the lower stratosphere and older age in the polar regions of the middle and upper stratosphere. The meridional and vertical gradients that characterize the age distribution in the stratosphere are the manifestation of barriers in transport. The average behavior of the transport barriers is diagnosed by means of the potential vorticity gradient. The simulated barriers in potential vorticity gradient in the lower-middle stratosphere are comparable to that deduced from European Centre for Medium-Range Weather Forecast reanalysis.

1. Introduction

Within the current global perspective the mean mass circulation that encompasses the middle atmosphere is characterized by ascent through the tropical tropopause into the stratosphere, poleward motion in the extratropics, and descent in the polar regions: the so-called Brewer-Dobson circulation of mass (for a review, see *Andrews et al.* [1987] and *Holton et al.* [1995]). During the solstitial seasons in the mesosphere the circulation consists of a single cell, with rising motion in the summer hemisphere, descending motion in the winter hemisphere, and meridional motion from the summer to the winter hemispheres: the Murgatroyd-Singleton circulation (see *McIntyre* [1992] for a review). On long timescales this circulation tends to produce a distribution of a tracer, of tropospheric origin, that peaks in the equatorial region of the middle stratosphere and decreases poleward in both hemispheres. The steepness of the tracer isolines in latitude (i.e., the meridional gradient of the tracer concentration) depends on the

opposite effects of quasi-isentropic planetary wave motions and mixing (that tends to flatten the isolines) and the Brewer-Dobson circulation (that tends to steepen the isolines). There is also increasing evidence that regions of the stratosphere are relatively isolated, at least seasonally. Such isolation has led to the concept of barriers to transport [*Plumb*, 1996], as the subtropical barriers observed in tracer concentrations (among others, *Trepte and Hitchman* [1992] and *Randel et al.* [1993]) and the winter polar vortex barriers associated with the resilience to transport of the Rossby wave restoring mechanism [*McIntyre*, 1992].

In this work, the large-scale transport in a middle atmosphere general circulation model is investigated and evaluated by analyzing a multiyear simulation that included a passive (chemically inert) tracer. The multiyear simulation has been performed by specifying surface emissions linearly increasing with time and aimed at representing the sources of sulphur hexafluoride, SF₆, a compound of anthropogenic origin. The SF₆ tracer is predominantly released in industrialized areas of the Northern Hemisphere, its main sources being leakages and degassing from high-voltage electrical equipment and metallurgy. The SF₆ tracer is of particular interest because of its very long lifetime (estimates range

Copyright 1999 by the American Geophysical Union.

Paper number 1999JD900963.
0148-0227/99/1999JD900963\$09.00

from 800 to 3200 years [Maiss *et al.*, 1996 and references therein]), and because there are no apparent sinks in the troposphere and stratosphere. The atmospheric concentration of SF₆ has increased from 0.03 pptv in 1970 to 3 pptv in 1993 [Maiss *et al.*, 1996; Maiss and Levin, 1994].

The evaluation of the large-scale transport of a middle atmosphere general circulation model is relevant to the coupling of general circulation models to models of the evolution of the chemical constituents of the atmosphere. Such model simulations are currently the tools for predicting environmental changes associated with anthropogenic changes of the atmospheric composition. Given that the evaluation of such highly interactive models can be complicated and blurred by unknown feedbacks among radiation, chemistry, and dynamics, a thorough evaluation of the simulated transport of a passive tracer can give confidence to the reliability of the general circulation model used. From the sensitivity of the residual circulation to planetary wave breaking and parameterized mesospheric gravity wave breaking, documented for instance by Manzini and McFarlane [1998] and Rind *et al.* [1999], it appears that models with large temperature biases may severely misrepresent the large-scale mass circulation. Other sources of uncertainty in transport characteristics include the horizontal and vertical resolutions and the numerical representation of the advection scheme.

2. Model and Design of the Experiment

The general circulation model used is the middle atmosphere MAECHAM4 model developed at the Max Planck Institute in Hamburg. It is an upward extended version of the ECHAM4 model. Most of the physical parameterizations, particularly those that are relevant mainly for tropospheric processes, and the basic model structure are common to both models. A detailed description of the ECHAM4 model is given by Roeckner *et al.* [1996a, b, and reference therein]. The major differences between the two models include the specification of the vertical coordinate and the location of the model top (ECHAM4 model, top at 10 hPa; MAECHAM4 model, top at 0.01 hPa), the parameterization of the effects of gravity waves, and a few modifications in the radiation scheme. The model structure and parameterizations are summarized by Manzini and McFarlane [1998] and Manzini *et al.* [1997].

Triangular spectral truncation at wave number 30 (T30 horizontal truncation) has been used in the current simulation. The sea surface temperature field is specified following the Atmospheric Model Intercomparison Project monthly mean climatology [Gates, 1992], the ozone distribution follows the monthly zonal mean from the chemical model of Brühl [1993], and the diurnal and seasonal cycles are included in the radiative transfer calculation.

In the MAECHAM4 model the gravity wave parameterization consists of two parts, separately representing the effects of the momentum deposition from orographic gravity waves and from a continuous gravity wave spectrum. A modified version of the McFarlane [1987] parameterization is used to account for the orographic gravity wave drag. The Doppler spread formulation of Hines [1997a, b] is used to parameterize the effects of a continuous spectrum of nonorographic gravity waves. The present configuration of the gravity wave source spectrum employed to initialize the Hines parameterization takes into account the results of Manzini and McFarlane [1998], where the middle atmosphere circulation was found to be sensitive to the launching height and, in turn, to the azimuthal distribution of the gravity wave momentum flux in the tropopause region. Given that knowledge of gravity wave sources from observations and theory is still limited, also in this simulation a relatively simple configuration is used. The spectrum is launched at a low level, just above the surface layer (third model level from the surface), with a root-mean-square (rms) wind speed of 1 ms⁻¹. This configuration is very similar to that used in their second simulation (EXP2) by Manzini and McFarlane [1998], but for a smaller gravity wave rms wind speed.

The 15-year ensemble zonal mean temperature for January and July from the MAECHAM4 model version used in this work is shown in Figure 1. A composite of the National Centers for Environmental Prediction - Climate Prediction Center (NCEP-CPC) [Randel, 1992] 15-year ensemble mean (pressures above 1 hPa) and the Cooperative Institute for Research in Atmosphere CIRA86 [Fleming *et al.*, 1990] standard atmosphere zonal mean temperature (pressures below 1 hPa) is also shown in Figure 1. In agreement with the NCEP-CPC analysis, the simulated mean temperature increases with height in the stratosphere, the warmest temperature being at the summer pole at the stratopause (260-270 K). In both January and July the polar temperature minimum associated with the winter polar night stratospheric jet is more pronounced in the model than in the NCEP-CPC data. This cold bias in July causes an upward shift of the warm stratopause at the South Pole, located between 60 and 70 km in the model instead of been confined to 60 km (compare with CIRA86). The reversal of the meridional temperature gradient between summer and winter in the upper mesosphere is captured by the model; the warmest temperatures are found at the winter pole at the mesopause, in agreement with the CIRA86 data, although quantitative biases are evident. Comparison of Figure 1 with the results of Manzini and McFarlane [1998 their Figure 6] shows that the current simulation is characterized by a temperature distribution in the winter hemisphere that is intermediate between their first simulation (CNTRL) and their EXP2 simulation, as expected from the results of the sensitivity to the configuration of the Hines pa-

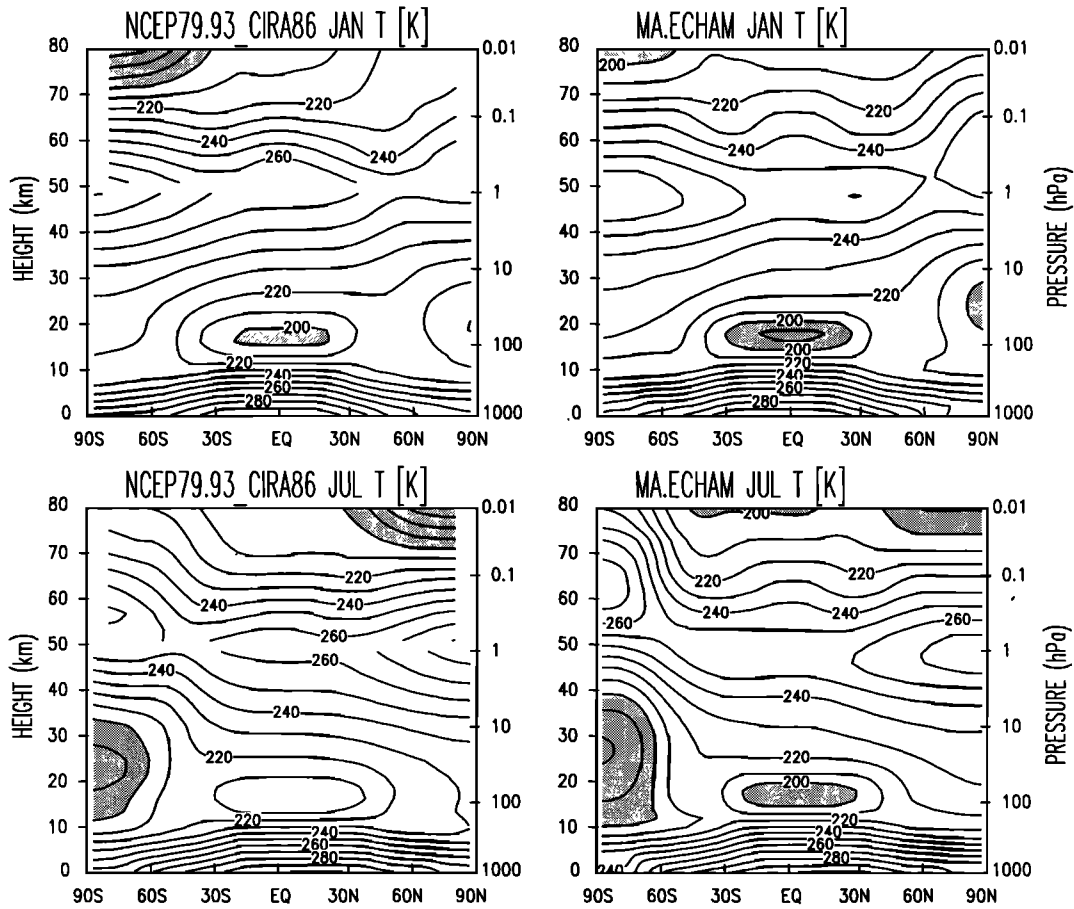


Figure 1. Zonal mean temperature: (right) ensemble mean from the 15-year simulation and (left) composite of the 15-year NCEP analysis (1979-1993) ensemble mean, pressures above 1 hPa, and the CIRA86 standard atmosphere, pressures below 1 hPa. January means are shown at top and July means at bottom. The contour interval is 10 K (shading indicates < 200 K).

rameterization. This is demonstrated quantitatively in Figure 2, where the latitude time evolution of the zonal mean temperature difference between the current model and the European Centre for Medium-Range Weather Forecast (ECMWF) reanalysis [Gibson *et al.*, 1997] is plotted at 100 and 30 hPa. A 30-day running mean, averaged over 15 years for the simulation and the reanalysis (1979-1993), is used to illustrate the low-frequency variability. The zonal mean temperature bias with respect to the ECMWF reanalysis is relatively small, typically much less than 5 K.

In the current simulation, SF₆ sources are specified at the surface, and emissions are linearly increasing with time. The annual global emission estimates from Levin and Hesshaimer [1996] are used, interpolated to monthly mean values. These global estimates are available from 1970 to 1993 and are geographically distributed according to electrical power usage as estimated by Denning *et al.* [1999]. Results are presented from a simulation that covers 15 years and 3 months; that is, the emission estimates from October 1970 to De-

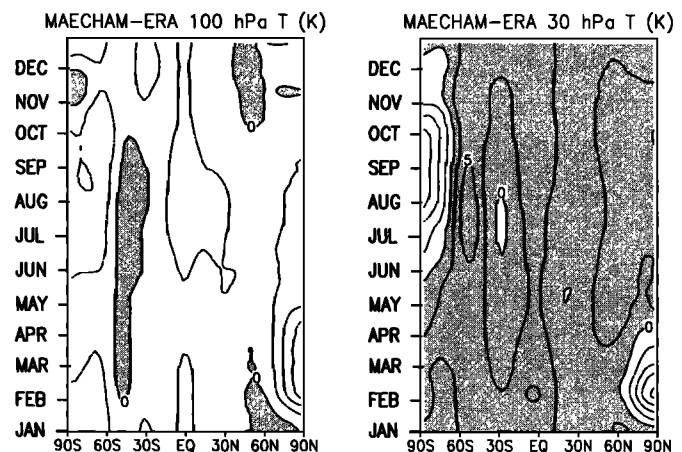


Figure 2. Difference between the simulation and the ECMWF reanalysis, MAECHAM4-ECMWF, for the 30-day running mean of the zonal mean temperature: latitude-time section (left) at 100 hPa and (right) at 30 hPa. Both fields are 15-year ensemble means (ECMWF: 1979-1993). The contour interval is 2.5 K (shading indicates positive values).

ember 1985 have been used. Chronology in the simulation is given only by the specified emission. The chemistry of SF₆ destruction is not well known, possible sinks appear to be associated with photochemical destruction confined to the mesosphere, and estimates of the SF₆ lifetime range from 800 to 3200 years [Maiss *et al.*, 1996, and references therein]. Given the present uncertainty in SF₆ chemistry, in the current simulation the mesospheric sinks of SF₆ are neglected. This assumption may, however, overestimate SF₆ concentration in the stratosphere, as pointed out by Hall and Waugh [1998]. Although SF₆ sinks appear to be confined to the mesosphere, Hall and Waugh [1998] have shown that the effect of the mesospheric chemical losses is transferred down to the stratosphere.

The period of the simulation, October 1970 to December 1985, covers the duration of Project AIRSTREAM part of the Environmental Measurements Laboratory (EML), consisting of SF₆ concentration measurements from aircraft sampling missions. Almost 1000 air samples were collected during the years 1973-1983 under project AIRSTREAM [Leifer, 1992]. SF₆ samples have been taken in the troposphere and lower stratosphere of the Northern and Southern Hemispheres, mainly in spring, summer, and fall. The latitude coverage extended from 75°N to 51°S. According to Leifer [1992] the sampling and analytical uncertainty of these data are better than 5%. These EML observations form a unique data set, as only very few observations of trace gases are available in the free troposphere and lower stratosphere and have been compared with more recent measurements [Maiss *et al.*, 1996]. Consequently, a scaling factor has been derived for the EML observations by I. Levin (personal communication, 1998) depending on which laboratory made the analysis. We applied these scaling factors, which are 1.18 for analysis performed by Health and Safety Laboratory (HASL), 1.52 for Washington State University (WSU), and 1.76 for Oregon Graduate Center (OGC), to the EML observations when comparing them to the model simulation results.

3. Comparison With SF₆ Observations

Measurements of long-term increase in SF₆ concentration from the Cape Grim (Tasmania, 41°S, 145°E) background air monitoring station [Maiss *et al.*, 1996] are plotted in Figure 3, together with model data at the corresponding grid point. The simulated SF₆ concentration at the beginning of the period considered is smaller than that measured. This underestimation is at least in part expected, given that a zero distribution has been used to initialize the tracer field in the model. A constant mixing ratio of 0.13 pptv has therefore been added to the model results in the following comparison with the EML observations. Figure 3 also shows that the simulated SF₆ increases in time to a somewhat faster rate (roughly 10% in 8 years), suggesting that the employed emission rate is slightly too large.

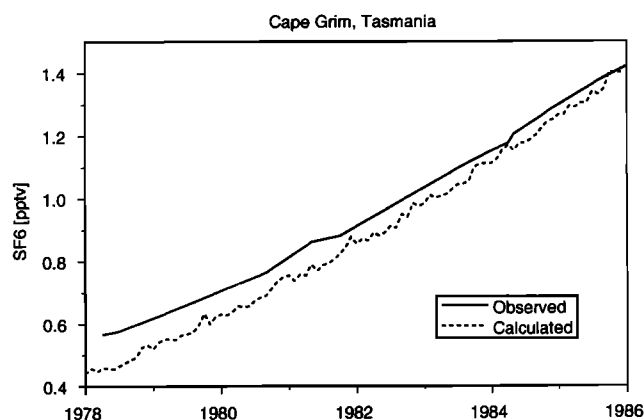


Figure 3. SF₆ concentration at the Cape Grim Station (Tasmania, 41°S, 145°E) (solid curve) and at the corresponding grid point from the model (dashed curve).

The detrended SF₆ concentrations from the EML data and the simulation are shown in Plate 1, binned according to latitude and distance from the tropopause. Both data sets have been detrended with respect to the global mass budget of 1978 (from the simulation). The year 1978 is chosen because it is in the middle of the observation record. The model data are monthly zonal means, selected for the month when the observations occurred. The EML data set is averaged over the available observations in each month and over the longitudes covered by the measurements. In Plate 1 all available months are plotted; the cover in latitude and height is therefore due to observations that occurred in different months. The EML data include the height of the tropopause derived from the observed temperature profiles. The model tropopause height has been determined by the lapse rate condition (lapse rate less than or equal to 2 K km⁻¹ [Holton *et al.*, 1995]). In general, the model tropopause is slightly higher than the observed tropopause, as might be expected by the model cold bias in the upper troposphere. The use of the tropopause is an attempt to use dynamical information in the diagnostic of tracer behavior.

The relative incoherence of the EML data, especially close to the tropopause, is presumably caused by variability in the meteorological synoptic systems, given that the observations lasted only a few minutes and covered a small range of longitudes. Nevertheless, the EML data exhibit a general tendency of high concentrations below and around the tropopause (0.5-0.7 pptv) and low concentrations (≤ 0.5 pptv) at high latitudes above the tropopause (lower stratosphere). The simulated SF₆ concentration is characterized by a much smoother tracer distribution. The low variability of the simulated SF₆ concentration is not surprising, given that the model data are monthly and zonal averages of grid point values, while the observations are averages of point measurements affected by the local and transient meteorological situation. It is therefore not possible to infer if there is a tendency to produce an ex-

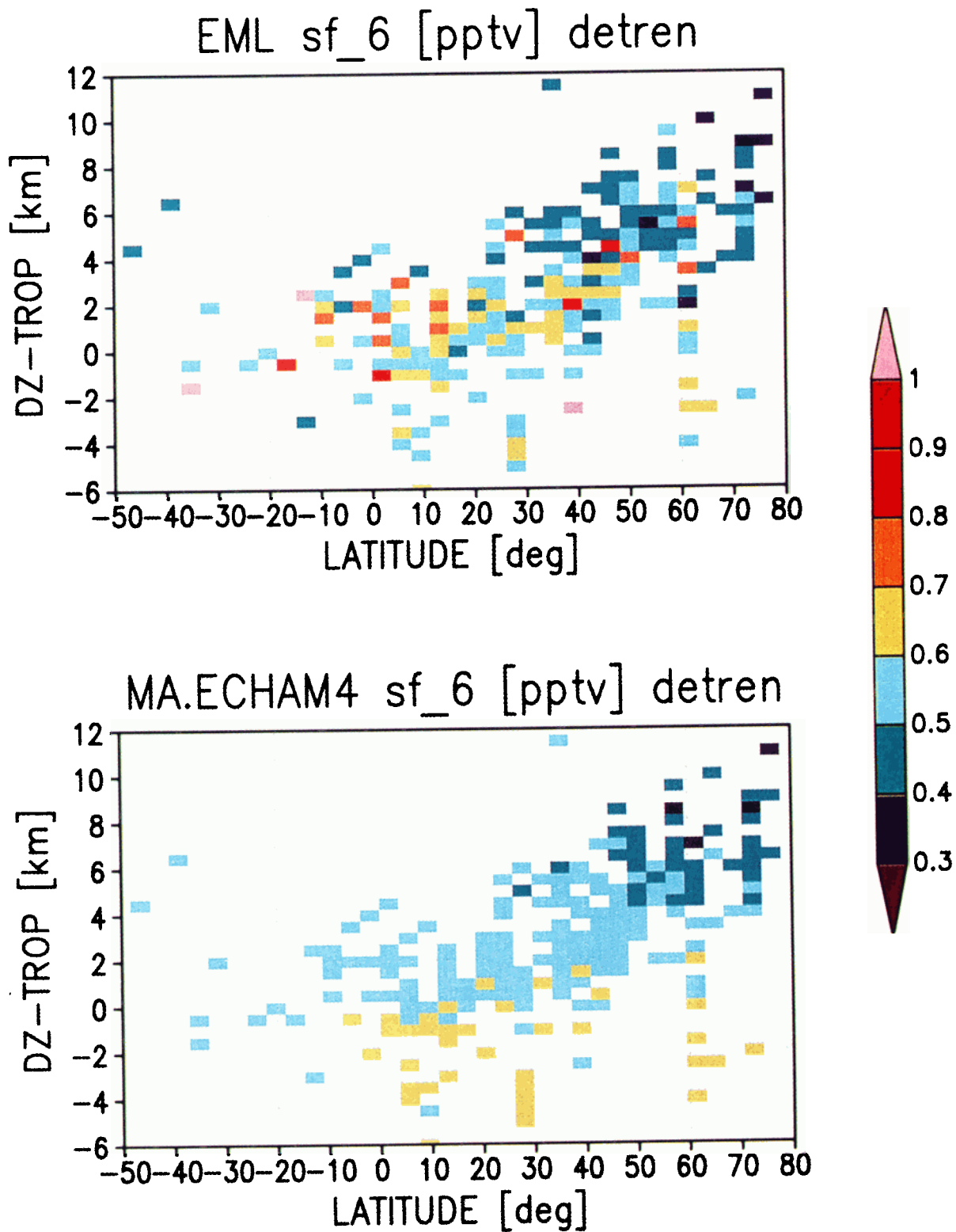


Plate 1. Detrended SF₆ concentration (pptv) binned according to latitude and distance (DZ) from tropopause: (top) EML observations and (bottom) model data. Both data sets have been detrended according to the global mass budget of 1978 (from the simulation).

cessively smoother field in the model from this comparison. The interesting result of Plate 1 is that the model data clearly show high (≥ 0.6 pptv) concentration below the tropopause and low (≤ 0.5 pptv) concentration at high latitudes in the lower stratosphere, reproducing the main features of the EML observations. Given that the data are detrended, the overall agreement means that the average transport is realistic in the model.

Figure 4 (top) shows the evolution in time of the SF₆ concentration for the EML measurements and model data at altitudes at least 2 km below the tropopause (same data sets as in Plate 1, but not detrended). The data are for all the available latitudes. Within the few years considered, there is a quite good agreement in the time evolution of the SF₆ concentrations from the EML data and the model data. Given that locations 2 km below the tropopause are representative of the troposphere where the trace gases are rapidly mixed and that most of the latitudes considered are in the Northern Hemisphere, the agreement means that the source specification used in the model is reasonably accurate (see also *Kjellström et al.* [1999])

Figure 4 (middle) is for locations at least 2 km above the tropopause. Given that most of the locations are from high latitudes, in this case the SF₆ concentration depends remotely on the surface sources. Most of the SF₆ reaching the lower stratosphere high latitudes has presumably traveled through the tropical troposphere, moved upward in the tropical lower stratosphere, and finally crossed to high latitudes. The agreement between EML data and model data in this case therefore suggests that transport timescales between remote regions in the model domain are realistically simulated and motivates the age of stratospheric air diagnostic carried out in section 4.

Figure 4 (bottom) shows the relative bias of modeled SF₆ concentration (mod) to observed SF₆ concentration (obs), $(\text{mod}-\text{obs})/(\text{mod}+\text{obs})$, as a function of latitude for stratospheric locations (at least 2 km above the tropopause) and tropospheric locations (at least 2 km below the tropopause). Given that the relative bias is everywhere < 0.3 , the model data are within a factor of 2 from the EML data. Figure 4 (bottom) also indicates that there is a tendency to underestimate the observed mixing ratios in the stratosphere and to slightly overestimate them in the troposphere. A reason could be a too small net transport into the stratosphere in the model, arising, for instance, from coarse horizontal and/or vertical resolution and limitations in the transport scheme.

4. Transport Timescale

The simulation with a general circulation model of a tracer with surface sources linearly increasing in time and no sinks allows derivation of the so-called age of stratospheric air, a transport timescale between different locations in the atmosphere, generally between a specific location in the troposphere and any other lo-

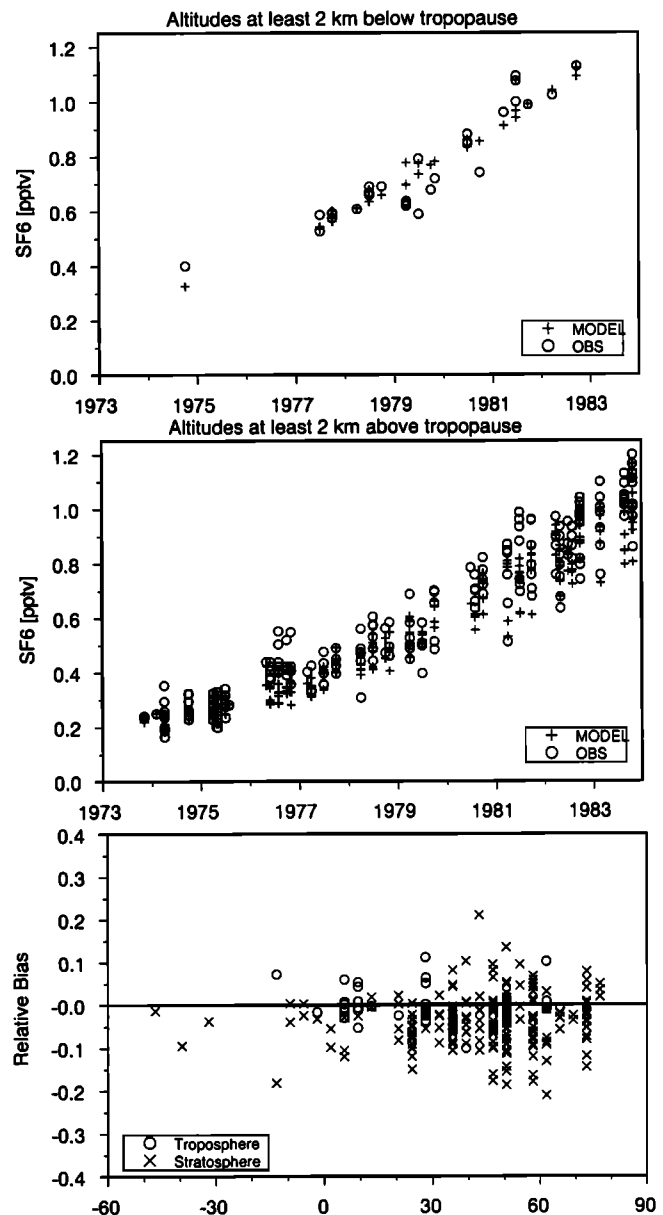


Figure 4. Comparison of SF₆ concentration (top) at altitudes at least 2 km below the tropopause and (middle) at altitudes at least 2 km above the tropopause (circles, EML observations; pluses, model data). (bottom) SF₆ relative bias $(\text{mod}-\text{obs})/(\text{mod}+\text{obs})$. Crosses give biases for stratospheric locations (at least 2 km above the tropopause) and circles for tropospheric locations (at least 2 km below the tropopause).

cation above. *Hall and Plumb* [1994] have discussed in detail the concept of age and derived an expression for the age of stratospheric air that takes into account the statistical nature of an air parcel. Estimates of the age of stratospheric air following *Hall and Plumb* [1994] have been extensively computed from chemical transport models, for instance by *Waugh et al.* [1997], *Hall and Waugh* [1998], and *Hall et al.* [1999]. *Waugh et al.* [1997] computed the age of stratospheric air from

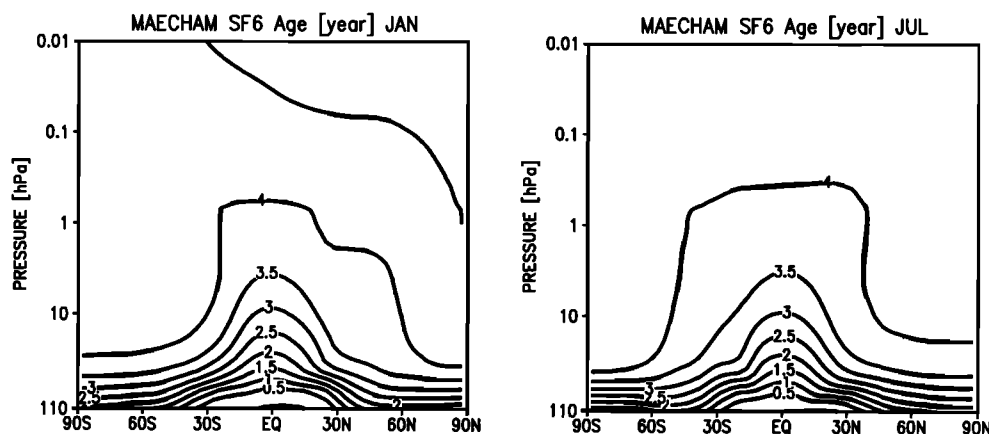


Figure 5. (left) January and (right) July zonal mean age of air between the equatorial tropopause and the domain above. The contour interval is 0.5 year.

a SF₆ simulation using winds from the Middle Atmosphere Community Climate Model 2 (MACCM2), *Hall and Waugh* [1998] evaluated the effects of a number of idealized mesospheric sinks on the stratospheric age distribution, and the recent work of *Hall et al.* [1999] presents an extensive comparison of age distributions from a number of stratospheric chemical transport models and a large number of measurements.

For the current SF₆ simulation the age of stratospheric air is computed following *Hall and Plumb* [1994]. This method can be used when changes in the emission can be detected in the higher part of the model domain, after at least 5-6 years from the initialization of the simulation. For the case in which the emissions increase linearly in time, the age of air is defined as the difference between the tracer mixing ratio at a reference point, usually the equatorial tropopause, and any other point above, divided by the growth rate at the reference point. Results presented here are for the last year of the simulation (year 15 from the initialization), and the reference point is the equator, at the 110 hPa level. An annual average growth rate at the reference point has been used, in order to eliminate spurious effects on the age computation due to the tropospheric annual cycle in the growth rate.

The age distribution in the middle atmosphere for January and July is shown in Figure 5. For both months the age distribution in the stratosphere is characterized by an increase in age with elevation and by a tropical bulge. In particular, the increase in age with elevation is rapid in the lower stratosphere (below 20 hPa). In the middle and upper stratosphere the increase in age is mainly confined to the tropics (especially in summer, while in winter, planetary wave breaking may flatten the age isolines; see the 4-year contour in January), thus enhancing the meridional gradient in the subtopo-

ics. The age distribution in Figure 5 is consistent with the established notion that on average, air enters the stratosphere from the tropical upper troposphere, and the simulated age distribution is in qualitative agreement with the general features of the age distribution inferred from a large number of observations by *Hall et al.* [1999]. Note that in the mesosphere the age distribution is quite uniform, indicating fast meridional and vertical transport, acting on a seasonal scale or less (the Murgatroyd-Singleton circulation). The mesospheric age distribution tends to a uniform value of ~ 4 -4.5 years.

For a more quantitative comparison with age estimates from observations reported by *Hall et al.* [1999], in Figure 6, selected meridional and vertical profiles of the age distribution for January are depicted. From Figure 6 (left) it appears that although in the tropics (5°S, dashed contour) there is a relatively fast increase in age from 100 to 20 hPa, the age is ~ 1 year younger at 10 hPa in comparison to that inferred from SF₆ measurements reported by *Hall et al.* [1999][see also *Harnisch et al.*, 1996; and *Patra et al.*, 1997]. At high latitudes (65°N, solid contour) the age vertical profile shows a rapid increase between 100 and 50 hPa in agreement with observations. However, in the middle and upper stratosphere the age values in Figure 6 are comparable only to estimates from sounding outside the polar vortex. Age from sounding inside the polar vortex is ~ 8 years (see again *Hall et al.* [1999] and *Harnisch et al.* [1996]), i.e., about a factor of 2 more than that computed from the MAECHAM4 simulation. A reason for such discrepancy could be, in part, that the age in Figure 6 is computed from a monthly mean, not necessarily representative of the transport situation inside the polar vortex. Downwelling of SF₆-poor air from the mesosphere may be responsible for the very old age inside the

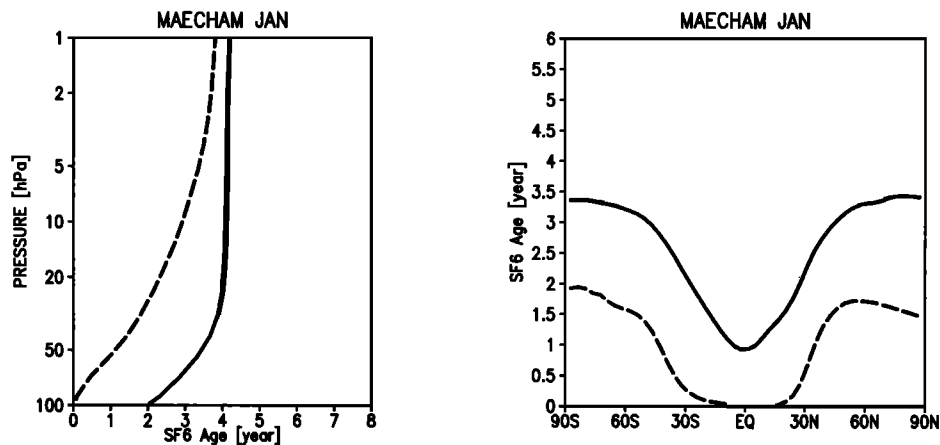


Figure 6. January zonal mean age of air between the equatorial tropopause and the domain above. (left) Vertical profiles at 5°S (dashed curve) and at 65°N (solid curve). (right) Meridional profiles at 54 hPa (solid curve) and at 110 hPa (dashed curve).

polar vortex estimated by *Harnisch et al.* [1996]. Moreover, younger age in the model might likely be caused by the absence of the mesospheric SF₆ sinks in the simulation. According to *Hall and Waugh* [1998] the absence of sinks in a model simulation could decrease the age up to 65% in the high-latitude middle stratosphere. The difference in the MAECHAM4 age with respect to estimates from observations could therefore be accounted for by the absence of sinks in the simulation.

Note that younger age in the polar stratosphere is not a consequence of the model cold bias. On the contrary, the cold bias may in fact give rise to older age, given that it is accompanied by a weaker residual circulation. A clear illustration of the relation between residual circulation and age is shown by *Hall et al.* [1999, figure 12], by whom the age distributions derived from two versions of the NCAR MACCM2 model are compared. *Hall et al.* [1999] show that a younger age distribution (a 2-year difference at 40 km) is obtained from the version of the NCAR MACCM2 model with stronger residual circulation. The difference in temperature structure and residual circulation simulated in July between the current MAECHAM4 and the MACCM2 models used *Waugh et al.* [1997] can also explain the younger age found in the current simulation in the upper stratosphere and mesosphere with respect to that shown in *Waugh et al.* [1997].

Figure 6 (right) indicates an increase with elevation of the age meridional gradient: At the 100 hPa level (dashed curve) the difference in age between the equatorial and high latitudes (at both sides of the equator) is ~ 1.5 years, while at the 54 hPa level (solid curve) a difference of ~ 2.5 years is found. The larger meridional gradient in age at 54 hPa is indicative of the tropical confinement of the rising air, associated with the existence of low-latitude transport barriers [*Plumb*, 1996; *Bowman and Hu*, 1997]. However, the comparison with

the observations reported by *Hall et al.* [1999] indicates that equatorward of 30° (both sides of the equator) the meridional age difference in MAECHAM4 is underestimated by ~ 0.5 -1 year.

5. Relation to Dynamical Fields

The meridional and vertical variations in the age distribution shown in section 4 are a manifestation of the existence of regions of weak transport in the stratosphere, the so-called transport barriers. Evidence of barriers in transport are given from observations [*Trepte and Hitchman*, 1992] and models, as, for instance, semi-Lagrangian computation of tracer evolution [*Chen et al.*, 1994]. Possible mechanisms for the existence of barriers are discussed by *Bowman* [1996] and *Bowman and Hu* [1997], among others.

The January zonal wind and meridional gradient of potential vorticity on the 600 K isentrope, 15-year ensemble mean from the ECMWF reanalysis, and 7-year ensemble mean from the model are depicted in Figure 7. The reanalysis data, originally at T106, were first spectrally truncated at T30, the model resolution, prior to the calculation of the potential vorticity and its gradient. The 7 years from the simulation are chosen from the time period for which the SF₆ data have been detrended, in order to show average behavior (see Figure 8). The 600 K isentrope is representative of the middle stratosphere, being located, on average, between 50 and 10 hPa. In the ECMWF data the polar night jet (strong westerlies) exhibits a zonal dependence due to the presence of quasi-stationary planetary waves; westerlies larger than 30 ms⁻¹ (shaded area in Figure 7) are found at 60°N between 60°W and 120°E and at higher latitudes in the Pacific sector. Weak westerlies or the presence of easterlies over the North Pacific at middle latitudes are associated with the Aleutian high,

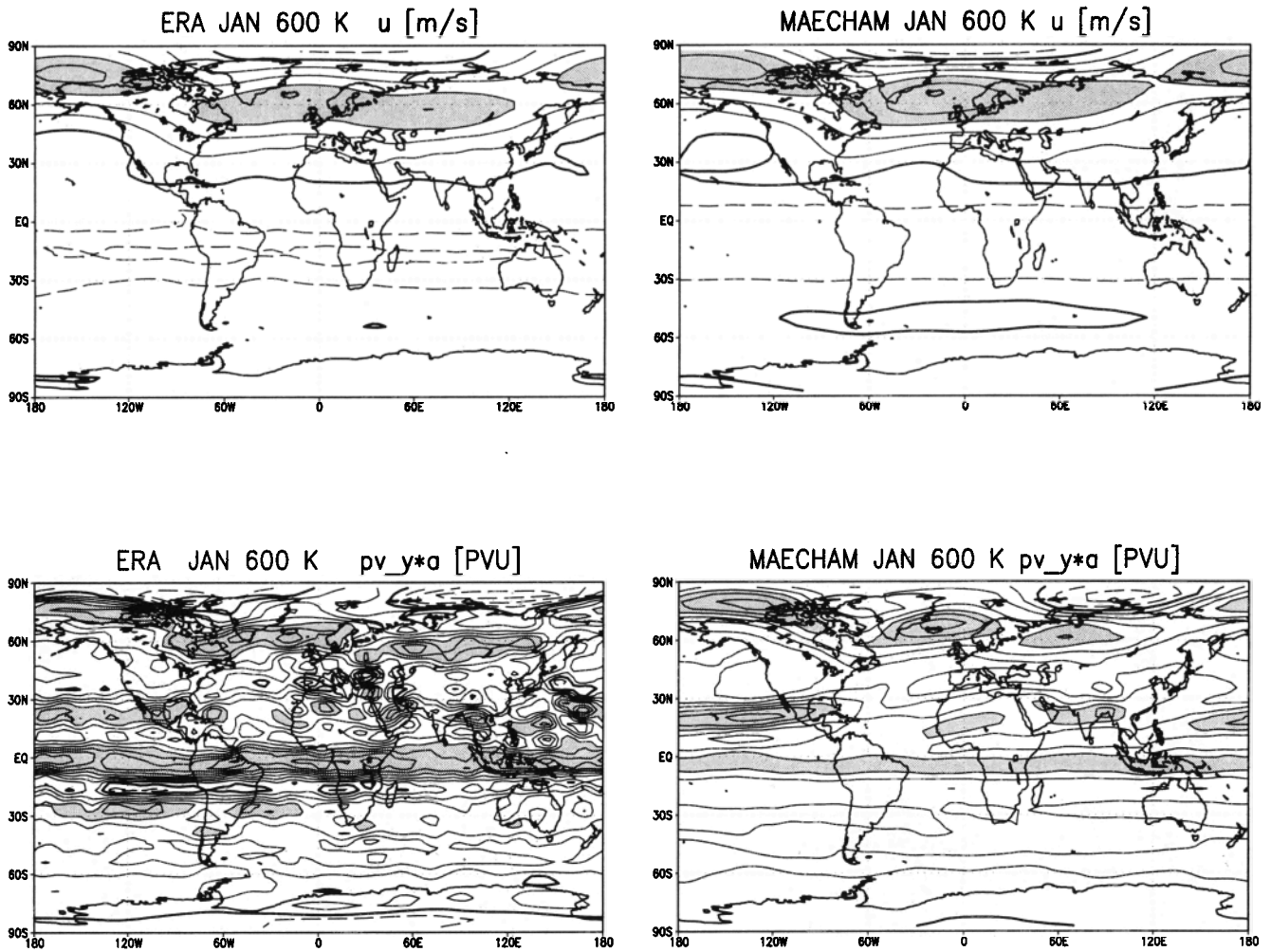


Figure 7. January ensemble mean (left) from 15-year ECMWF reanalysis (1979-1993) and (right) from 7 years of the 15-year simulation. (top) Zonal wind at 600 K; the contour is 10 m s^{-1} (shading indicates $> 30 \text{ m s}^{-1}$). (bottom) Meridional gradient of potential vorticity times the radius of the Earth ($a=6.671 \times 10^6 \text{ m}$) at 600 K; the contour is 30 PVU (shading indicates $> 120 \text{ PVU}$).

a typical climatological feature of the northern winter stratosphere [Harvey and Hitchman, 1996]. The average latitudinal and zonal location and the strength of the polar night jet and the weak winds associated with the Aleutian high are well simulated in the model. The simulated westerlies are, however, slightly stronger over the North Atlantic. A reason for stronger winds could be a relatively short averaging period (7 years); middle atmospheric models are known to present large interannual variability [see, e.g., Boville, 1995; Hamilton, 1995; Manzini and Bengtsson, 1996].

From Figure 7 (bottom) it clearly appears that the ECMWF and the simulated polar night jets (northern high latitudes) are respectively associated with latitudinal bands of strong meridional gradient of potential vorticity, as highlighted by the shading. In particular, strong gradients are found over the North Atlantic, Eurasia, and poleward of 60°N elsewhere, while regions

of weak gradient appear equatorward of the polar night jet. Quantitatively, there is a good agreement between the ECMWF and model results, although the overall picture is a much noisier ECMWF field. The small-scale structures in the reanalysis are evidence of inconsistency in the observations.

The regions of weak gradient in potential vorticity are the manifestation of quasi-isentropic planetary wave breaking and large-scale irreversible mixing (transient formation and breaking off of large potential vorticity undulations are occasionally found in the model). These regions of weak gradient are the so-called surf regions [McIntyre and Palmer, 1983, 1984].

In the northern subtropics, at the southern edges of the north Pacific mixing region (south of 30°N , between 180°W and 60°W), another clearly defined band of strong gradient is found, in both the ECMWF reanalysis and the model results. Other localized bands

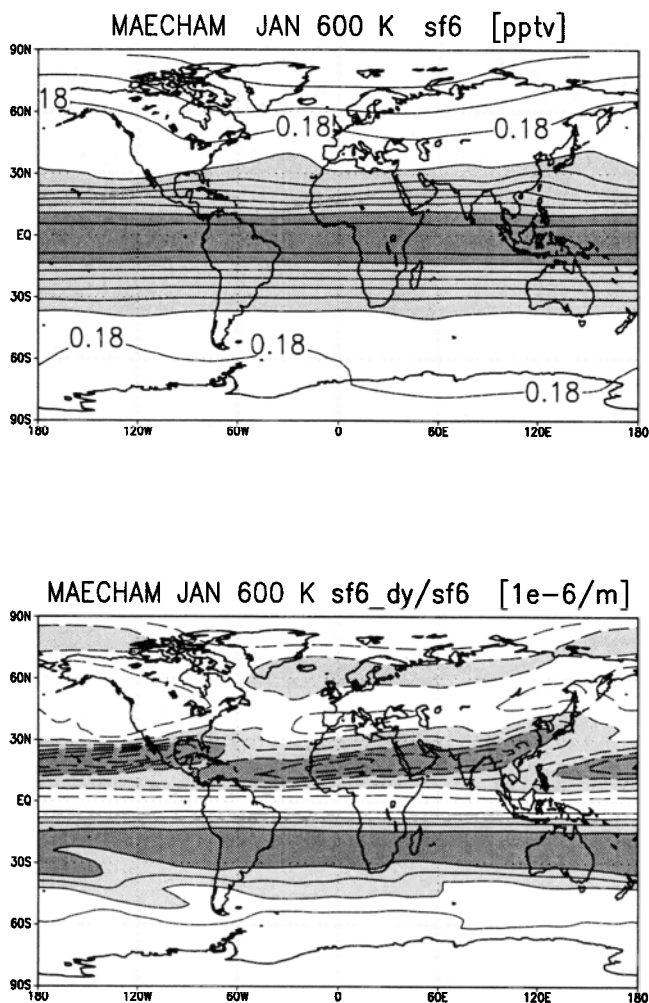


Figure 8. January ensemble mean at 600 K from 7 years of the 15-year simulation. (top) Detrended SF₆ concentration (pptv); the contour is 0.02 pptv (light shading indicates > 0.2 pptv, and dark shading > 0.3 pptv). (bottom) Detrended meridional SF₆ relative change (meridional gradient of concentration over concentration); the contour is $0.04 \times 10^{-6} \text{ m}^{-1}$ (light shading indicates $> 0.08 \times 10^{-6} \text{ m}^{-1}$ and $< -0.08 \times 10^{-6} \text{ m}^{-1}$; dark shading indicates $> 0.16 \times 10^{-6} \text{ m}^{-1}$, and $< -0.16 \times 10^{-6} \text{ m}^{-1}$).

over North Africa and Asia are clearly seen in the model but only hinted at in the noisy reanalysis data.

In the Southern (summer) Hemisphere there is little structure in the meridional potential vorticity gradient field. The polar barrier and midlatitude planetary wave breaking are, in fact, seasonal features, present in the winter hemisphere when westerlies dominate the large-scale stratospheric circulation and planetary waves can propagate upward from the troposphere where they are generated. The equatorial band of strong gradient seen in Figure 7 is associated with the change in sign of potential vorticity between the hemispheres.

The 7-year January ensemble mean of the detrended SF₆ concentration and the detrended meridional relative change in SF₆ concentration at 600 K are shown

in Figure 8. The tracer concentration is largest along the equator and sharply decreases poleward. These features are consistent with the age diagnostic presented before and the notion that tropospheric air enters the stratosphere in the equatorial region, a feature generally captured by stratospheric transport models [Hall et al., 1999].

The barriers deduced from the SF₆ relative change reproduce those deduced from the potential vorticity gradient in the Northern Hemisphere: The undulating high-latitude barrier to transport associated with the polar night jet and the subtropical barrier, with local maxima over the Pacific and Africa (highlighted by light and dark shading in Figure 8). The comparison of the potential vorticity gradient (Figures 7) with the SF₆ relative change (Figure 8) shows that breaks or weakening in either the potential vorticity gradient or the SF₆ relative change tend to occur in the northern subtropics over the Atlantic and far east Asia - west Pacific, suggesting that these geographical locations could be preferred regions of tropical-extratropical exchange. Consistent with this interpretation is the observation of an event of a tongue of dry air emanating from the tropical Atlantic during northern winter [Randel et al., 1993].

Figure 8 in addition shows that a subtropical barrier occurs also during summer (Southern Hemisphere), manifested by the large relative change in SF₆ at $\sim 20^\circ\text{S}$; but not evident in the potential vorticity gradient (although there are hints of it). Tropical confinement during summer has been found in previous simulations of tracer transport [Chen et al., 1994; Bowman and Hu, 1997].

In summary, from the diagnosis of the relative change in SF₆ the average subtropical barrier appears in both summer and winter, an indication of the role of the residual circulation, given a long-lived tracer of tropospheric origin. During summer a plausible reason for the existence of the subtropical barrier is the lack of large-scale mixing due to the predominant easterlies in the stratosphere. The band of large relative change in SF₆ (dark shading in Figure 8) is indeed poor in zonally varying features. However, during winter the large-scale mixing does not appear to break down the subtropical barrier on average, with the exceptions of the localized areas noted above (Atlantic and far east Asia). On the contrary, sharp tracer gradients are found at the equatorward side of the mixing regions, consistent with the potential vorticity gradient depicted in Figure 7.

Concerning the examination of the large-scale transport in the simulation, the potential vorticity gradient has disclosed the effects of the local dynamics (direct effect of planetary wave breaking) on the large-scale transport. The latitudinal relative change of the SF₆ concentration has in addition revealed the nonlocal effects of planetary and gravity wave dynamics (indirect effect via the residual circulation) in the summer hemisphere.

6. Summary and Conclusions

A 15-year simulation with the MAECHAM4 general circulation model of a passive tracer with emissions aimed at representing those of the SF₆ tracer of anthropogenic origin has been performed. The MAECHAM4 model uses the Hines parameterization of the momentum flux deposition due to a broad gravity wave spectrum [Manzini *et al.*, 1997 and Manzini and McFarlane, 1998]. The configuration of the gravity wave source spectrum used in the Hines parameterization in the present model is a compromise aimed at limiting the cold bias in the winter stratosphere of each hemisphere, without sophisticated ad hoc specification of the gravity wave sources, as exemplified in the simulated climatological temperature structure.

Comparisons of the simulated SF₆ concentration with EML measurements (from project AIRSTREAM) have shown a good agreement between detrended concentrations, characterized by comparably high values in the upper troposphere and low values in the lower stratosphere. Consistent rate of increase with time of the simulated SF₆ concentration and of the concentration deduced from the EML measurements in the troposphere indicates that sources have been correctly represented in the model. The SF₆ relative bias indicates that there is a tendency to underestimate the observed concentration in the stratosphere while overestimating it in the troposphere.

The large-scale transport in the middle atmosphere reproduced by the model as revealed by the simulation of the SF₆ tracer (long-lived tracer of tropospheric origin) is consistent with expectation from theory, observations, and previous modeling work. High concentrations of SF₆ are found in the equatorial lower-middle stratosphere. Average barriers to meridional transport highlighted by large gradients in the averaged fields of potential vorticity and detrended SF₆ concentration have been found along the polar night jet, at the equatorward edge of planetary wave mixing regions in winter and in the subtropics in summer. Given the quantitative agreement with the potential vorticity gradient computed from the ECMWF reanalysis, the Northern Hemisphere regions of weak and strong mixing are apparently well simulated in the model. Given the lack of global observations of SF₆, it is at this stage not possible to quantify the summer subtropical barrier directly.

The simulated large-scale transport has also been diagnosed by computing the age of air deduced from the time evolution of the SF₆ concentration. It has been found that the simulated vertical structure of the age distribution in the tropical lower-to-middle stratosphere is in reasonably good agreement with estimates from observations [Harnisch *et al.*, 1996; Hall *et al.*, 1999]. In summary, it has been shown that (1) a sharp increase in age occurs in the lower stratosphere; (2) in the tropics the age of air is ~4 years in the upper stratosphere; (3) the polar regions of the stratosphere are characterized

by older age, and therefore they are relatively remote to tropospheric air; and (4) the mesosphere is characterized by a uniform age distribution of ~4-4.5 years.

The age of stratospheric air is a transport diagnostic sensitive to the mean meridional circulation: Therefore it can be used as an indirect diagnostic of the mechanical dissipation (for instance, that produced by a gravity wave parameterization) occurring in a general circulation model, as exemplified by the comparison of the results presented here with those presented by Waugh *et al.* [1997] and Hall *et al.* [1999], and the sensitivity simulations performed with the Goddard Institute for Space Studies (GISS) general circulation model and reported by Rind *et al.* [1999].

Ongoing and future work concerning further evaluation of the transport in the MAECHAM model suite include evaluation of the sensitivity to the vertical and horizontal resolutions and to the transport scheme as well as the diagnosis and evaluation of transient events of large-scale quasi-isentropic mixing spontaneously occurring in the simulation.

Acknowledgments. The authors would like to thank L. Bengtsson for support and encouragement, M. Giorgetta for providing the code for the isentropic diagnostics, D. Waugh and E. Kjellström for providing respective manuscripts prior to publication, K. Winger for assembling the EML data, R. Leifer and I. Levin for providing the emission and EML data, and U. Schlese for technical assistance. Valuable reviews from A. Plumb and S. Pawson and constructive comments from L. Bengtsson, C. Brühl, and D. Waugh all contributed to improve the manuscript and are gratefully acknowledged. This work was supported by projects IGWOC (contract ENV4-CT97-0486) and SINDICATE (contract ENV4-CT97-0483) of the European Commission Environment and Climate Research Programme.

References

- Andrews, D. G., J. R. Holton, and C. B. Leovy, *Middle Atmospheric Dynamics*, 489 pp., Academic, San Diego, Calif., 1987.
- Boville, B. A., Middle atmosphere version of the CCM2 (MACCM2): Annual cycle and interannual variability, *J. Geophys. Res.*, **100**, 9017-9039, 1995.
- Bowman, K. P., Rossby wave phase speeds and mixing barriers in the stratosphere. Part I: Observations, *J. Atmos. Sci.*, **905-916**, 1996.
- Bowman, K. P., and Y. Hu, Tropical mixing barriers in the lower stratosphere in the Geophysical Fluid Dynamics Laboratory SKYHI model, *J. Geophys. Res.*, **102**, 21,465-21,478, 1997.
- Brühl, C., Atmospheric effects of stratospheric aircraft, in *Models and Measurements Workshop*, edited by M. Prather and E. Remsberg, *NASA Ref. Publ. 1292 II*, 1993.
- Chen, P., J. Holton, A. O'Neill, and R. Swinbank, Isentropic mass exchange between the tropics and extratropics in the stratosphere, *J. Atmos. Sci.*, **51**, 3006-3018, 1994.
- Denning, A. S., et al., Three-dimensional transport and concentration of SF₆: A model intercomparison study (TansCom2), *Tellus*, in press, 1999.
- Fleming, E. L., S. Chandra, J. J. Barnett, and M. Corney, Zonal mean temperature, pressure, zonal wind and geopotential height as functions of latitude, *Adv. Space Res.*, **10**, 1211-1259, 1990.

- Gates, W. L., AMIP: The atmospheric model intercomparison project, *Bull. Am. Meteorol. Soc.*, *73*, 1962-1970, 1992.
- Gibson, J. K., P. Kallberg, S. Uppala, A. Hernandez, A. Nomura, and E. Serrano, ERA description, *ECMWF Re-Anal. Proj. Rep. Ser. 1*, Eur. Cent. for Medium-Range Weather Forecast, Reading, England, 1997.
- Hall, T. M., and R. A. Plumb, Age as a diagnostic of stratospheric transport, *J. Geophys. Res.*, *99*, 1059-1070, 1994.
- Hall, T. M., and D. W. Waugh, Influence of nonlocal chemistry on tracer distributions: Inferring the mean age of air from SF₆, *J. Geophys. Res.*, *103*, 13,327-13,336, 1998.
- Hall, T. M., D. W. Waugh, K. A. Boering, and R. A. Plumb, Evaluation of transport in stratospheric models, *J. Geophys. Res.*, *104*, 18,815-18,839, 1999.
- Hamilton, K., Interannual variability in the Northern Hemisphere winter middle atmosphere in control and perturbed experiments with the GFDL SKYHI general circulation model, *J. Atmos. Sci.*, *52*, 44-66, 1995.
- Harnisch, J., R. Borchers, P. Fabian, and M. Maiss, Tropospheric trends for CF₄ and C₂F₆ since 1982 derived from SF₆ dated stratospheric air, *Geophys. Res. Lett.*, *23*, 1099-1102, 1996.
- Harvey, V. L., and M. H. Hitchman, A climatology of the Aleutian High, *J. Atmos. Sci.*, *53*, 2088-2101, 1996.
- Hines, C. O., Doppler spread parameterization of gravity wave momentum deposition in the middle atmosphere. Part 1: Basic formulation, *J. Atmos. Sol. Terr. Phys.*, *59*, 371-386, 1997a.
- Hines, C. O., Doppler spread parameterization of gravity wave momentum deposition in the middle atmosphere. Part 2: Broad and quasi monochromatic spectra and implementation, *J. Atmos. Sol. Terr. Phys.*, *59*, 387-400, 1997b.
- Holton, J. R., P. H. Haynes, M. E. McIntyre, A. R. Douglass, R. B. Rood, and L. Pfister, Stratosphere-troposphere exchange, *Rev. Geophys.*, *33*, 403-439, 1995.
- Kjellström, E., J. Feichter and G. Hoffmann, Transport of SF₆ and ¹⁴CO₂ in the atmospheric general circulation model ECHAM4, *Tellus*, in press, 1999.
- Leifer, R., Project AIRSTREAM: Trace gas final report, *EML-549*, 162 pp., U.S. Dep. of Energy, New York, 1992.
- Levin, I., and V. Hesshaimer, Refining of atmospheric transport model entries by the globally observed passive tracer distributions of ⁸⁵Kr and SF₆, *J. Geophys. Res.*, *101*, 16,745-16,755, 1996.
- Maiss, M., and I. Levin, Global increase of SF₆ observed in the atmosphere, *Geophys. Res. Lett.*, *21*, 569-572, 1994.
- Maiss, M., L. P. Steele, R. J. Francey, P. J. Fraser, R. L. Langenfelds, N. B. A. Trivett, and I. Levin, Sulfur hexafluoride: A powerful new atmospheric tracer, *Atmos. Environ.*, *30*, 1621-1629, 1996.
- Manzini, E., and L. Bengtsson, Stratospheric climate and variability from a general circulation model and observations, *Clim. Dyn.*, *12*, 615-639, 1996.
- Manzini, E., and N. A. McFarlane, The effect of varying the source spectrum of a gravity wave parameterization in a middle atmosphere general circulation model, *J. Geophys. Res.*, *103*, 31,523-31,539, 1998.
- Manzini, E., N. A. McFarlane, and C. McLandress, Impact of the Doppler spread parameterization on the simulation of the middle atmosphere circulation using the MAECHAM4 general circulation model, *J. Geophys. Res.*, *102*, 25,751-25,762, 1997.
- McFarlane, N. A., The effect of orographically excited gravity wave drag on the general circulation of the lower stratosphere and troposphere, *J. Atmos. Sci.*, *44*, 1775-1800, 1987.
- McIntyre, M. E., Atmospheric dynamics: Some fundamentals, with observational implications, in *The Use of EOS for Studies of Atmospheric Physics*, edited by J. C. Gille and G. Visconti, *Proc. Int. Sch. Phys. Enrico Fermi*, 313-386, 1992.
- McIntyre, M. E., and T. N. Palmer, The "surf zone" in the stratosphere, *J. Atmos. Terr. Phys.*, *46*, 825-849, 1984.
- McIntyre, M. E., and T. N. Palmer, Breaking planetary waves in the stratosphere, *Nature*, *305*, 593-600, 1983.
- Patra, P. K., S. Lal, B. H. Subbaraya, C. H. Jackman, and P. Rajaratnam, Observed vertical profile of sulphur hexafluoride (SF₆) and its atmospheric applications, *J. Geophys. Res.*, *102*, 8855-8859, 1997.
- Plumb, R. A., A "tropical pipe" model of stratospheric transport, *J. Geophys. Res.*, *101*, 3957-3972, 1996.
- Randel, W. J., Global atmospheric circulation statistic, 1000-1 mb, *Tech. Rep. TN-366+STR*, Nat. Cent. for Atmos. Res., Boulder, Colo., 1992.
- Randel, W. J., J. C. Gille, A. E. Roche, J. B. Kumer, J. L. Mergenthaler, J. W. Waters, E. F. Fishbein, and W. A. Lahoz, Stratospheric transport from the tropics to middle latitudes by planetary-wave mixing, *Nature*, *365*, 533-535, 1993.
- Rind, D., J. Lerner, K. Shah, and R. Suozzo, Use of on-line tracers as a diagnostic tool in general circulation model development, 2, Transport between the troposphere and the stratosphere, *J. Geophys. Res.*, *104*, 9151-9167, 1999.
- Roeckner, E., K. Arpe, L. Bengtsson, M. Christoph, M. Claussen, L. Dümenil, M. Esch, M. Giorgetta, U. Schlese, and U. Schulzweida, The atmospheric general circulation model ECHAM4: Model description and simulation of present-day climate, *MPI rep. 218*, Max Planck Institut, Hamburg, Germany, 1996a.
- Roeckner, E., J. M. Oberuber, A. Bacher, M. Christoph, and I. Kirchner, ENSO variability and atmospheric response in a global coupled atmosphere-ocean GCM, *Clim. Dyn.*, *12*, 734-754, 1996b.
- Trepte, C. R. and M. H. Hitchman, Tropical stratospheric circulation deduced from satellite aerosol data, *Nature*, *355*, 626-628, 1992.
- Waugh, D. W., et al., Three-dimensional simulations of long-lived tracers using winds from MACCM2, *J. Geophys. Res.*, *102*, 21,493-21,513, 1997.

J. Feichter and E. Manzini, Max Planck Institut für Meteorologie, Bundesstrasse 55, 20146 Hamburg, Germany. (e-mail: feichter@dkrz.de; manzini@dkrz.de)

(Received April 13, 1999; revised July 19, 1999; accepted August 31, 1999.)